Inorganic Chemistry
Article

Inorg. Chem. **2010**, *49*, 3121–3129 **3121**
DOI: 10.1021/ic901546t

A Unique Nickel System having Versatile Catalytic Activity of Biological Significance

Tanmay Chattopadhyay,[†,▽] Madhuparna Mukherjee,[†] Arindam Mondal,[‡] Pali Maiti,[†] Arpita Banerjee,[†] Kazi Sabnam Banu,[†] Santanu Bhattacharya,[§] Bappaditya Roy,[‡] D. J. Chattopadhyay,[‡] Tapan Kumar Mondal,[∥] Munirathinam Nethaji,[⊥] Ennio Zangrando,[*,#] and Debasis Das[*,†]

[†]*Department of Chemistry, University of Calcutta, 92, A. P. C. Road, Kolkata-700 009, India,* [‡]*Dr. B. C. Guha Centre for Genetic Engineering and Biotechnology, University of Calcutta, Kolkata-700 019, India,* [§]*Department of Chemistry, Maharaja Manindra Chandra College, Kolkata-700 003, India,* [∥]*Department of Chemistry, Jadavpur University, Jadavpur, Kolkata-700 032, India,* [⊥]*Department of Inorganic and Physical Chemistry, Indian Institute of Science, Bangalore 560012, India, and* [#]*Dipartimento di Scienze Chimiche, University of Trieste, Via L. Giorgieri 1, 34127 Trieste, Italy.* [▽]*Present address: Nanotube Research Centre (NTRC), AIST, Tsukuba Central 5, 1-1-1 Higashi, Tsukuba, Ibaraki 305-805, Japan.*

Received August 4, 2009

A new dinuclear nickel(II) complex, $[Ni_2(LH_2)(H_2O)_2(OH)(NO_3)](NO_3)_3$ (**1**), of an "end-off" compartmental ligand 2,6-bis(*N*-ethylpiperazine-iminomethyl)-4-methyl-phenolato, has been synthesized and structurally characterized. The X-ray single crystal structure analysis shows that the piperazine moieties assume the expected chair conformation and are protonated. The complex **1** exhibits versatile catalytic activities of biological significance, viz. catecholase, phosphatase, and DNA cleavage activities, etc. The catecholase activity of the complex observed is very dependent on the nature of the solvent. In acetonitrile medium, the complex is inactive to exhibit catecholase activity. On the other hand, in methanol, it catalyzes not only the oxidation of 3,5-di-*tert*-butylcatechol (3,5-DTBC) but also tetrachlorocatechol (TCC), a catechol which is very difficult to oxidize, under aerobic conditions. UV−vis spectroscopic investigation shows that TCC oxidation proceeds through the formation of an intermediate. The intermediate has been characterized by an electron spray ionizaton-mass spectrometry study, which suggests a bidentate rather than a monodentate mode of TCC coordination in that intermediate, and this proposition have been verified by density functional theory calculation. The complex also exhibits phosphatase (with substrate *p*-nitrophenylphosphate) and DNA cleavage activities. The DNA cleavage activity exhibited by complex **1** most probably proceeds through a hydroxyl radical pathway. The bioactivity study suggests the possible applications of complex **1** as a site specific recognition of DNA and/or as an anticancer agent.

Introduction

In spite of the very rich coordination chemistry of nickel, its biological significance is not well developed. All types of nickel enzymes known to date are of plant or bacteria origins.[1−8] Here, it is noteworthy that it had taken about 50 years to identify the first nickel metalloenzyme since the date of crystallization (1926)[9] of jack-bean urease, the first enzyme ever isolated as a crystalline material.[10] The aspects pointed out above lead to at least two considerations: first, it is premature to exclude the possible presence of a nickel enzyme in animals, and second, the apparent lack of interest to explore the biochemistry of nickel. During the past few years, we have been interested in searching for small coordination molecules that exhibit enzymatic activity to mimic the structure as well as the functional properties of metallobiosites. Our recent work on the dinuclear Cu^{II}-system (here system stands for the "end-off" compartmental ligand

*To whom correspondence should be addressed. E-mail: dasdebasis2001@yahoo.com.

(1) Walsh, C. T.; Orme-Johnson, W. H. *Biochemistry* **1987**, *26*, 4901.
(2) *The Bioinorganic Chemistry of Nickel*; Lancaster, J. R., Jr., Ed.; VCH: New York, 1988.
(3) Nickel and its role in biology. In *Metal Ions in Biological systems*; Sigel, H., Ed.; Marcel Dekker: New York, 1988; Vol. *23*.
(4) Haussinger, R. P. Biochemistry of nickel. In *Biochemistry of the Elements*, Frieden, E., series Ed.; Plenum Press: New York, 1993; Vol. *12*.
(5) Cammack, R.; van Vliet, P. Catalysis by nickel in biological system. In *Bioinorganic Catalysis*; Redijik, J., Bouernans, L., Eds.; Marcel Dekker: New York, 1998.
(6) Maroney, M. J.; Davidson, G.; Allan, C. B.; Figlar, J. *Struct. Bonding* (*Berlin*) **1998**, *92*, 1.
(7) Fontecilla-Camps, J. C. *Struct. Bonding* (*Berlin, Ger.*) **1998**, *91*, 1.
(8) Ragsdale, W. S. *Curr. Opin. Chem. Biol.* **1998**, *2*, 208.
(9) Sumner, J. B. *J. Biol. Chem.* **1926**, *69*, 435.
(10) Jabri, E.; Carr, M. B.; Hausinger, R. P.; Karplus, P. A. *Science* **1995**, *268*, 998.

© 2010 American Chemical Society
Published on Web 03/01/2010

2,6-bis(*N*-ethylpiperazine-iminomethyl)-4-methyl-phenol, LH) enabled us to find out the most active model of catechol oxidase known to date.[11] It not only catalyzes the oxidation of 3,5-di-*tert*-butylcatechol (3,5-DTBC) to 3,5-di-*tert*-butylbenzoquinone (3,5-DTBQ) (with a k_{cat} value as high as 2.88×10^4 h^{-1}) but also that of tetrachlorocatechol (TCC) to tetrachlorobenzoquinone (TCQ), a process never reported earlier by using dinuclear copper(II)-complexes. In this paper, we report the synthesis and the comprehensive characterization by routine physicochemical studies and by X-ray single crystal structure analysis of a unique dinuclear nickel(II) complex $[Ni_2(LH_2)(H_2O)_2(OH)(NO_3)](NO_3)_3$, **1**, having the same compartmental ligand. The complex, besides being a model compound for the *met* form of the active site of catechol oxidase, it exhibits a broad spectrum of catalytic activities of biological significance, in particular, it catalyzes the hydrolysis reaction of the phosphate monoester *p*-nitrophenylphosphate (PNPP) and causes the cleavage in plasmid DNA.

Experimental Section

Physical Methods and Materials. All materials were obtained from commercial sources and used as purchased. Solvents were dried according to standard procedure and distilled prior to use. The 2,6-diformyl-4-methylphenol was prepared according to the literature method.[12] Nickel nitrate hexahydrate (Merck) and *N*-(2-aminoethyl)piperazine (Aldrich) were purchased from commercial sources and used as received. Nickel was estimated gravimetrically with dimethylglyoxime. Elemental analyses (carbon, hydrogen, and nitrogen) were performed using a Perkin-Elmer 240C analyzer. Infrared spectra (4000−400 cm^{-1}) were recorded at 28 °C on a Shimadzu FTIR-8400S using KBr as a medium. Electronic spectra (800−200 nm) were obtained at 27 °C using a Shimadzu UV-3101PC, where dry acetonitrile/dry methanol were used as a medium as well as a reference. The electrospray mass spectra were recorded on a MICROMASS Q-TOF mass spectrometer. The electron paramagnetic resonance (EPR) experiment was done at both 25 and −135 °C in pure methanol using a Bruker EMX-X band diffractometer. The measurements of the variable-temperature magnetic susceptibility and the field dependence of magnetization were carried out on a Quantum Design MPMS-XL5 SQUID magnetometer. Susceptibility data was collected using an external magnetic field of 0.2 T in the temperature range of 2−300 K. The experimental susceptibilities were corrected for diamagnetism (Pascal's tables).[13]

Experimental Procedure of the 3-(4,5-dimethylthiazol-2-yl)-2,5-diphenyl tetrazonium bromide (MTT) Assay. Monkey kidney fibroblast (VERO) cells and A549 cells (a carcinomas human alveolar basal epithelial cell line) were maintained in Dulbecco's modified eagle medium (DMEM) media supplemented with 5% (v/v) calf serum, 2 mmol/L glutamine, and 1% (v/v) penicillin (streptomycin).Cells (T-25 flask) were cultured at 37 °C in a humid atmosphere containing 5% CO_2 and subcultured every 2−3 days. Cells were harvested with trypsin, and a suspension containing 2×105 cells per mL was prepared. This assay was performed in a 96-well, flat-bottomed, γ-irradiated, microliter plates with lids. Filter sterilized (0.22 μM), phosphate buffer saline (PBS) soluble complex **1** (1 mg/mL) (50 μL) was serially diluted. Both negative (50 μL PBS) and positive controls (50 μL Triton X-100) were included. Cells were grown in the wells for 24 h, up to 70−80% confluence. The wells were then inoculated aseptically with 50 μL of different dilutions of the samples and the negative and positive controls, and the plates were incubated at 37 °C in a humid atmosphere containing 5% CO_2 for 30 h. After the incubation period, 50 μL of an aqueous solution of MTT (2 mg/mL) was added to each well, and the plates were incubated further for 4 h at 37 °C in a humid atmosphere containing 5% CO_2. After this time, the liquid medium in the wells was removed, 200 μL of dimethylsulfoxide (DMSO) was added to each well, and the absorbance at 450 nm was determined in a microplate reader. The toxic effect of complex **1** on the VERO cell line was calculated from the following (eq 1):

$$\%\text{viability} = (\text{mean absorbance of the sample}/\text{mean absorbance of the control}) \times 100 \quad (1)$$

Table 1. Crystallographic Data and Details of Refinement for Complex **1**

empirical formula	$C_{21}H_{40}N_{10}Ni_2O_{16}$
formula weight	806.05
crystal system	hexagonal
space group	$P6_1$
a (Å)	9.9402(13)
c (Å)	57.2290(15)
volume (Å^3)	4897.1(9)
Z	6
calc density (g/cm^3)	1.640
M (Mo−Kα) (mm^{-1})	1.240
F(000)	2520
θ range (°)	2.14−27.98°
collected reflections	12 428
indep reflections	4948
*R*int	0.0604
observed reflections $I > 2\sigma(I)$	3112
parameters	458
$R1$ $[I > 2\sigma(I)]$	0.0531
$wR2$ $[I > 2\sigma(I)]$	0.0737
goodness of fit on F^2	0.885
residuals (e Å^{-3})	0.463, −0.359

X-ray Data Collection and Crystal Structure Determination. Diffraction data for the structure reported were collected at room temperature on a BRUKER SMART APEX diffractometer (Mo−Kα radiation, $\lambda = 0.71073$ Å) equipped with a charge-coupled device (CCD). Cell refinement and indexing and scaling of the data sets were carried out using packages Bruker SMART APEX and Bruker SAINT.[14] The structure was solved by direct methods and subsequent Fourier analyses[15] and refined by the full-matrix least-squares method based on F^2 with all observed reflections. The contribution of hydrogen (H) atoms at calculated positions was introduced in the final cycles of refinement. Crystallographic data and details of refinement are reported in Table 1. All the calculations were performed using the WinGX System, version 1.70.01.[16]

Synthesis of Complex 1. A methanolic solution (5 mL) of *N*-(2-aminoethyl)piperazine (0.258 g, 2 mmol) was added dropwise to a heated methanolic solution (10 mL) of 2,6-diformyl-4-methylphenol (0.164 g, 1 mmol), and the resulting mixture was boiled for 30 min. Then, a methanolic solution (15 mL) of $Ni(NO_3)_2 \cdot 6H_2O$ (0.673 g, 2.5 mmol) was added, and the resulting mixture was refluxed for two hours. After cooling, the clear deep-green solution was kept in a $CaCl_2$ desiccator in the dark. Rectangular-shaped blue crystals of **1**, suitable for X-ray data collection, were obtained after a few days. Yield: 0.48 g (72%). FT-IR: ν(C=N) 1621 cm^{-1}; ν(skeletal vibration) 1546 cm^{-1};

(11) Banu, K. S.; Chattopadhyay, T.; Banerjee, A.; Bhattacharaya, S.; Suresh, E.; Nethaji, M.; Zangrando, E.; Das, D. *Inorg. Chem.* **2008**, *47*, 7083.
(12) Gagne, R. R.; Spiro, C. L.; Smith, T. J.; Hamann, C. A.; Thies, W. R.; Shiemeke, A. K. *J. Am. Chem. Soc.* **1981**, *103*, 4073.
(13) (a) Dutta, R. L.; Syamal, A. *Elements of Magnetochemistry*, 2nd ed.; East West Press: Manhattan Beach, CA, 1993. (b) Kahn, O. *Molecular Magnetism*; VCH : New York, 1993.
(14) *SMART, SAINT Software Reference Manual Bruker*; Bruker AXS Inc.: Madison, WI, 2000.
(15) Sheldrick, G. M. *SHELX97 Programs for Crystal Structure Analysis* (*Release 97-2*); University of Göttingen: Göttingen, Germany, 1998.
(16) Farrugia, L. J. *J. Appl. Crystallogr.* **1999**, *32*, 837.

$\nu(H_2O)$ 3399.4 cm^{-1}. UV−vis (MeOH)/nm: 395 (sh, ε = 6728 $M^{-1}cm^{-1}$), 599 (sh, ε = 1040 $M^{-1}cm^{-1}$), 968 (sh, ε = 402 $M^{-1}cm^{-1}$). Anal. calcd for $C_{21}H_{40}N_{10}O_{16}Ni_2$: C, 31.26; H, 4.96; N, 17.37; Ni, 14.56%. Found: C, 31.36; H, 4.73; N, 17.39; Ni, 14.58%.

Computational Details. Density functional theory (DFT) calculations were carried out with the Gaussian 03 package.[17] The exchange functional of Becke and the correlation functional of Lee, Yang, and Parr (B3LYP)[18,19] were employed in combination with the Stuttgart−Dresden (SDD) effective core potentials[20] for the Ni atoms and the 6-31G(d) basis set[21] for the remaining elements. Frequency calculations were performed within the harmonic approximation to check whether the optimized geometries correspond to energy minima (NIMAG = 0) on the potential energy surface. The J value for **1** was calculated following the previously reported method,[22] using the broken-symmetry approach to estimate the energy of the low-spin states. We have used $H = -2JS_1S_2$ convention for the exchange Hamiltonian, the equation for calculating the J value is $J = [E(QT) - E(BSS)]/6$, where $E(QT)$ is the energy of the quintet state of the dinuclear Ni complex and $E(BSS)$ is the energy of its broken-symmetry singlet state. Vertical electronic excitations based on UB3LYP optimized geometry were computed using the time-dependent density functional theory (TD-DFT) formalism[23] in methanol using a conductor-like polarizable continuum model (CPCM).[24]

Results and Discussion

Description of Crystal Structure. The X-ray structural determination of compound **1** reveals a dinuclear nickel cationic complex and a nitrate anion. An ORTEP view of μ-phenoxo-dinickel(II) complex of **1** with an atom labeling scheme is shown in Figure 1. The nickel ions exhibit a distorted octahedral coordination sphere comprised in the equatorial plane of the phenoxido-bridged oxygen, the hydroxyl group, and the imine and amine nitrogen donors. The axial positions are occupied by an aqua and a nitrate oxygen. The Ni−N(amine) bond distances (2.218(5), 2.231(6) Å) are significantly longer than the Ni−N(imine) ones (2.011(5), 2.004(6) Å), and the Ni−O bond lengths appear slightly shorter for the phenoxido oxygen when compared with the hydroxyl group (2.043(4) vs 1.996(5) Å, mean values). On the other hand, the axial $Ni-ONO_2$ and $Ni-OH_2$ distances average to 2.161(5) and 2.106(6) Å, respectively. The bond angles Ni(1)−O(1)−Ni(2) and Ni(1)−O(2)−Ni(2) of 93.26(17) and 96.2(2)°, respectively, lead to an intermetallic separation of 2.970(1) Å (see Table 2). The piperazine moieties assume the expected chair conformation and are protonated, as deduced for the charge balance and the occurrence of H-bond distances. The crystal packing shows an extended H-bonding scheme (see Supporting Information). In fact, protonated piperazine nitrogens and coordinated water molecules, acting as H-donors toward nitrate anions, lead to a three-dimensional (3D) supramolecular arrangement.

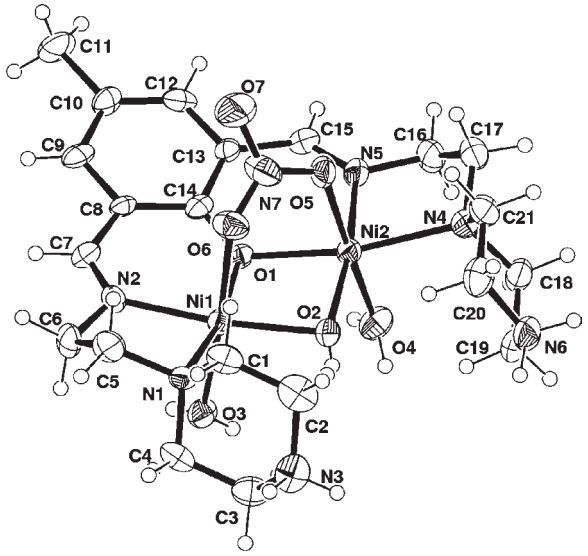

Figure 1. ORTEP view of the cationic dinuclear complex of **1**.

Table 2. Selected Coordination Bond Lengths (Angstroms) and Angles (Degrees) for **1** with Esds in Parentheses

Ni(1)−N(1)	2.218(5)	Ni(2)−N(4)	2.231(6)
Ni(1)−N(2)	2.011(5)	Ni(2)−N(5)	2.004(6)
Ni(1)−O(1)	2.039(4)	Ni(2)−O(1)	2.047(4)
Ni(1)−O(2)	1.995(5)	Ni(2)−O(2)	1.996(5)
Ni(1)−O(3)	2.104(5)	Ni(2)−O(4)	2.109(6)
Ni(1)−O(6)	2.185(5)	Ni(2)−O(5)	2.138(5)
Ni(1)−Ni(2)	2.970(1)		
N(2)−Ni(1)−N(1)	83.2(2)	N(5)−Ni(2)−N(4)	83.4(2)
O(1)−Ni(1)−N(1)	169.30(19)	O(1)−Ni(2)−N(4)	169.1(2)
O(2)−Ni(1)−N(1)	104.1(2)	O(2)−Ni(2)−N(4)	104.7(2)
O(3)−Ni(1)−N(1)	93.0(2)	O(4)−Ni(2)−N(4)	92.9(2)
O(6)−Ni(1)−N(1)	87.12(19)	O(5)−Ni(2)−N(4)	86.2(2)
N(2)−Ni(1)−O(1)	88.36(19)	N(5)−Ni(2)−O(1)	88.31(19)
O(2)−Ni(1)−N(2)	171.9(2)	O(2)−Ni(2)−N(5)	171.9(2)
N(2)−Ni(1)−O(3)	88.1(2)	N(5)−Ni(2)−O(4)	86.8(2)
N(2)−Ni(1)−O(6)	88.3(2)	N(5)−Ni(2)−O(5)	88.5(2)
O(2)−Ni(1)−O(1)	84.0(2)	O(2)−Ni(2)−O(1)	83.79(18)
O(1)−Ni(1)−O(3)	93.3(2)	O(1)−Ni(2)−O(4)	93.6(2)
O(1)−Ni(1)−O(6)	86.05(19)	O(1)−Ni(2)−O(5)	86.56(17)
O(2)−Ni(1)−O(3)	94.95(19)	O(2)−Ni(2)−O(4)	92.2(2)
O(2)−Ni(1)−O(6)	88.53(19)	O(2)−Ni(2)−O(5)	92.62(19)
O(3)−Ni(1)−O(6)	176.4(2)	O(4)−Ni(2)−O(5)	175.2(2)

Magnetic Study. The variable temperature magnetic data of the complex were collected on a polycrystalline sample in the temperature range of 300−2 K, using an

(17) Frisch, M. J.;Trucks, G. W.; Schlegel H. B.; Scuseria G. E.; Robb, M. A.; Cheeseman, J. R.; Montgomery, J. A., Jr.; Vreven, T.; Kudin, K. N.; Burant, J. C.; Millam, J. M.; Iyengar, S. S.; Tomasi, J.; Barone, V.; Mennucci, B.; Cossi, M.; Scalmani, G.; Rega, N.; Petersson, G. A.; Nakatsuji, H.; Hada, M.; Ehara, M.; Toyota, K.; Fukuda, R.; Hasegawa, J.; Ishida, M.; Nakajima, T.; Honda, Y.; Kitao, O.; Nakai, H.; Klene, M.; Li, X.; Knox, J. E.; Hratchian, H. P.; Cross, J. B.; Bakken, V.; Adamo, C.; Jaramillo, J.; Gomperts, R.; Stratmann, R. E.; Yazyev, O.; Austin, A. J.; Cammi, R.; Pomelli, C.; Ochterski, J. W.; Ayala, P. Y.; Morokuma, K.; Voth, G. A.; Salvador, P.; Dannenberg, J. J.; Zakrzewski, V. G.; Dapprich, S.; Daniels, A. D.; Strain, M. C.; Farkas, O.; Malick, D. K.; Rabuck, A. D.; Raghavachari, K.; Foresman, J .B.; Ortiz, J. V.; Cui, Q.; Baboul, A.G.; Clifford, S.; Cioslowski, J.; Stefanov, B. B.; Liu, G.; Liashenko, A.; Piskorz, P.; Komaromi, I.; Martin, R. L.; Fox, D. J.; Keith, T.; M. A. Al- LahamPeng, C. Y.; Nanayakkara, A.; Challacombe, M.; Gill, P. M. W.; Johnson, B.; Chen, W.; Wong, M. W.; Gonzalez, C.; Pople, J. A. *Gaussian 03*, Revision D.01; Gaussian, Inc., Wallingford CT, 2004.

(18) Becke, A. D. *Phys. Rev. A: At., Mol., Opt. Phys.* **1988**, *38*, 3098.

(19) Lee, C.; Yang, W.; Parr, R. G. *Phys. Rev. B: Condens. Matter* **1988**, *37*, 785.

(20) Dolg, M.; Wedig, U.; Stoll, H.; Preuss, H. *J. Chem. Phys.* **1987**, *86*, 866.

(21) Petersson, G. A.; Al-Laham, M. A. *J. Chem. Phys.* **1991**, *94*, 6081.

(22) Ruiz, E.; Rodriguez-Fortea, A.; Cano, J.; Alvarez, S.; Alemany, P. *J. Comput. Chem.* **2003**, *24*, 982.

(23) (a) Stratmann, R. E.; Scuseria, G. E.; Frisch, M. J. *J. Chem. Phys.* **1998**, *109*, 8218. (b) Casida, M. E.; Jamorski, C.; Casida, K. C.; Salahub, D. R. *J. Chem. Phys.* **1998**, *108*, 4439.

(24) (a) Barone, V.; Cossi, M. *J. Phys. Chem. A* **1998**, *102*, 1995. (b) Cossi, M.; Barone, V. *J. Chem. Phys.* **2001**, *115*, 4708. (c) Cossi, M.; Rega, N.; Scalmani, G.; Barone, V. *J. Comput. Chem.* **2003**, *24*, 669.

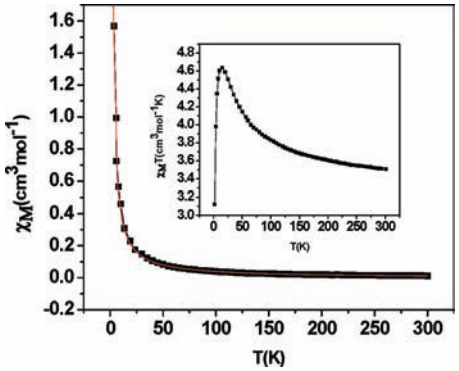

Figure 2. χ_M versus T plot of complex **1** and the χ_MT versus T plot is shown in inset. The solid line represents the theoretical curve using the equation for Ni_2 dimer.

applied magnetic field of 0.2 T. The plots of χ_M and χ_MT versus T data are shown in Figure 2. The χ_MT value at 300 K for the dimeric complex is 3.4 cm^3 mol^{-1} K, which is slightly higher than the theoretical value (3.0 cm^3 mol^{-1} K) for two noninteracting ions of a $S = 1$ spin state. The χ_MT value gradually increases upon decreasing temperature and reaches a maximum (4.65 cm^3 mol^{-1} K) at 10 K. Further cooling resulted in a sudden drop in χ_MT values. The room temperature χ_MT value as well as the increasing nature of the χ_MT values with decreasing temperature is a clear signature of the presence of a global ferromagnetic interaction in the molecule. The decrease of the χ_MT value at a temperature below 10 K is probably due to zero-field splitting and to intermolecular antiferromagnetic interaction.

To fit the magnetic susceptibility versus T data, we first attempted using a simple model of the dimer with a $S = 1$ spin state without considering zero-field splitting. The quality of fitting was not satisfactory, particularly in the low-temperature region. However, reasonable fitting was obtained when we considered the zero-field splitting, and the best-fitting parameters obtained were $g = 2.2$, $J = 44.26$ cm^{-1}, and $D = -4.6$ cm^{-1}. A similar magneto-structural correlation for the dinuclear nickel(II) complexes have been reported by some other groups.[25]

The singly occupied molecular orbitals (SOMOs) obtained by the ROB3LYP level calculation (see Supporting Information) reveal that they are essentially dz^2 and dx^2-y^2 characters with reduced contribution from the bridging μ-oxo, μ-phenoxido, and μ-NO_3 groups. The Mulliken spin density plot obtained by the UB3LYP level calculation (Figure 3) also clearly indicates the ferromagnetic interaction between the two Ni(II) centers is a superexchange phenomenon through the μ-oxo and μ-phenoxido groups, and the J value obtained from the calculation is 47.2 cm^{-1} with a slight overestimation from the experimental value (J_{exp} = 44.26 cm^{-1}).

Electronic Spectra and TD-DFT Calculation. In MeOH, complex **1** exhibits a moderately intense transition at 395 nm (ε, 6728 $M^{-1}cm^{-1}$) and a very weak shoulder at 599 nm (ε, 1040 $M^{-1}cm^{-1}$). In addition, one moderately intense shoulder at 968 nm (ε, 402 $M^{-1}cm^{-1}$) has been resolved. To predict the nature of electronic transitions, a UB3LYP/

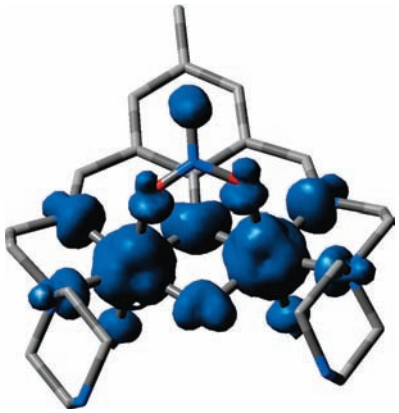

Figure 3. Spin density plot (isosurface cutoff value = 0.003).

TD-DFT calculation has been performed on the optimized structure of **1** in MeOH, and the calculated transitions are observed to match well with the experimental bands (Table 3). The calculation predicts low-energy transitions at 937.6 nm (f, 0.0058), 921.8 nm (f, 0.0037), 644.2 (f, 0.0045), and 618.4 (f, 0.0034). All these transitions correspond to a mixed d−d (Ni($d\pi$) → Ni($d\pi$)) and to a ligand to metal charge transition, LMCT, (L → Ni($d\pi$)) with a partially mixed metal to ligand charge transfer, MLCT (see Supporting Information). The transitions with a high oscillatory factor (f) at 426.3 nm (f, 0.0151) and 412.9 nm (f, 0.0185) correspond to a LMCT and an intraligand charge transfer transition (ILCT).

Catechol Oxidase Activity. The catecholase activity of complex **1** was evaluated by using 3,5-DTBC and TCC molecules as substrates. The reactions were carried out in two different solvents, methanol and acetonitrile, at 25 °C in aerobic conditions and were monitored by means of UV−vis spectroscopy, following the same technique as we reported earlier.[11] To our surprise, in the acetonitrile medium, complex **1** is observed to be completely inactive toward the oxidation of both of the substrates. On the other hand, in methanol, the oxidation of 3,5-DTBC proceeds very smoothly and exhibits a saturation kinetics (k_{cat} = 14 400 h^{-1}) (see Supporting Information). More interestingly, complex **1** catalyzes the oxidation of TCC to TCQ, a process never reported for any nickel system, and the process is observed via the formation of an intermediate (Figure 4).

The crystal structure analyses of **1** and of the analogous copper derivative[11] show that, due to protonation, positive charge centers are created on the piperazine nitrogen atoms at the two sides of the compartmental ligand. The extraordinary activity of the two above-mentioned complexes generates an inquiry as to whether these positive-charged centers may act as a channel to drive the catechol moieties, thereby inducing an unprecedented catecholase activity. A similar scheme was proposed in literature to explain the activity of CuZn−superoxide dismutase (SOD), where the Cu^{II} lies at the bottom of a narrow channel, and

(25) (a) Nanda, K. K.; Das, R.; Thompson, L. K.; Venkatsubramanian, K.; Paul, P.; Nag, K. *Inorg. Chem.* **1994**, *33*, 1188. (b) Koga, T.; Furutachi, H.; Nakamura, T.; Fukita, N.; Ohba, M.; Takahashi, K.; Okawa, H. *Inorg. Chem.* **1998**, *37*, 989.

(26) Tainer, J. A.; Getzoff, E. D.; Richardson, J. S.; Richardson, D. C. *Nature* **1983**, *306*, 284.

(27) Valentine, J. S.; Pantoliano, M. W. Protein-Metal ion interaction in Cuprozinc Protein (Superoxide dismutase) (R). In *Copper Proteins*; Spiro, T. G., Ed.; Krieger Publishing Co.: Malabar, FL, 1981, p. 291.

(28) Valentine, J. S.; Mota de Freitas, D. *J. Chem. Educ.* **1985**, *62*, 990.

Table 3. Selected Visible Energy Transitions at the TD-DFT/UB3LYP Level for **1**

energy (ev)	wavelength (nm)	osc. factor (*f*)	principal transitions	character	exp. value (ε, $M^{-1}cm^{-1}$)
1.3224	937.59	0.0058	(31%) 144(β) → 151(β) (29%) 142(β) → 152(β)	Ni(dπ) → Ni(dπ) L → Ni(dπ)	968(402)
1.3450	921.80	0.0037	(33%) 144(β) → 152(β) (28%) 142(β) → 151(β)	Ni(dπ) → Ni(dπ) L → Ni(dπ)	
1.9246	644.23	0.0045	(35%) 138(β) → 152(β) (28%) 142(β) → 152(β)	Ni(dπ) → Ni(dπ) L → Ni(dπ)	599(1040)
2.0050	618.39	0.0034	(39%) 145(β) → 152(β) (31%) 145(β) → 155(β)	Ni(dπ) → Ni(dπ) Ni(dπ) → L(π*) L → Ni(dπ) L → L(π*)	
2.9084	426.30	0.0151	(34%) 150(β) → 153(β) (28%) 150(β) → 156(β)	L(π) → L(π*) L(π) → Ni(dπ)	395(6728)
3.0025	412.94	0.0185	(39%) 150(β) → 152(β) (33%) 150(β) → 156(β)	L(π) → L(π*) L(π) → Ni(dπ)	

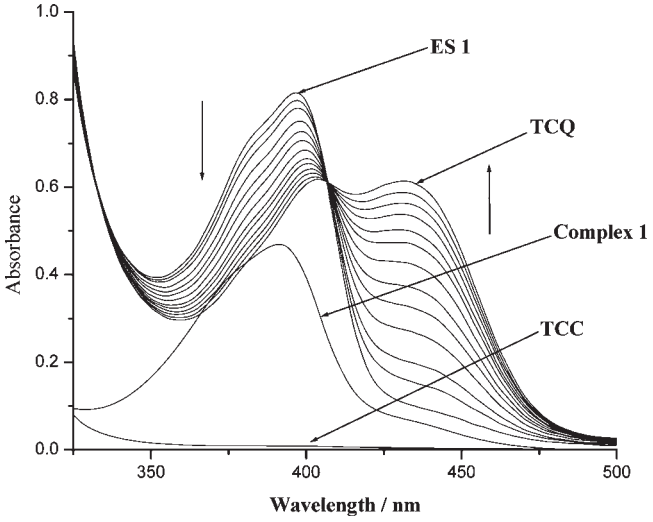

Figure 4. UV−vis spectra (300−500 nm): (i) **1** (1×10^{-4}M) in methanol; (ii) TCC (1×10^{-2}M) in methanol; (iii) changes in UV−vis spectra of **1** upon addition of 100-fold TCC observed after each 10 min interval.

the positively charged arginine and lysine residues are believed to play a role in attracting the anions and guiding them into the channel.[26−29] Further work is required to clarify these aspects. Another important issue we should address here is the role of the solvent on the catecholase activity of our complexes. Our present study reveals that methanol is a better choice to study the catecholase activity of the dinickel(II) complex rather than acetonitrile. At present, we believe that the higher the coordination ability of the solvent, the lower the catecholase activity of a catalyst in that solvent and that is most likely due to the competitive reaction between the solvent and the substrate to make an association with the catalyst. Since acetonitrile has a higher coordination ability than methanol, the coordinated water molecules of complex **1** may be substituted by acetonitrile in the solution, and the resultant species has little affinity to interact with the substrate, to exhibit any catalytic activity. However, on comparing the catalytic efficiency (on the basis of k_{cat} value) of complex **1** with its analogous copper(II) complex (Complex **2** in Table 4) for both of the substrates 3,5-DTBC and TCC, as depicted in Table 4, it may be stated that under identical conditions

(29) Bannister, J. V.; Bannister, W. H.; Rotilio, G. Aspects of the Structure, Function and Applications of Superoxide dismutase (R). *CRC Crit. Rev. Biochem*, **1987**, *22*, 111.

Table 4. Comparison of Catecholase Activity of Complex **1** with an Analogous Copper Complex

		substrate		
complex	solvent	3, 5-DTBC	TCC	k_{cat} (h^{-1})
1	MeOH	√	—	1.44×10^4
1	MeOH	—	√	0.339×10^4
2	MeOH	√	—	3.24×10^4
2	MeOH	—	√	1.04×10^4

the dicopper(II) system exhibits much better catecholase activity than that of the dinickel(II) system.

In order to understand the structure of the intermediate, we have performed an electron spray ionizaton-mass spectrometry (ESI-MS) study. The ESI-MS spectrum of **1** in methanol shows the base peak at 581.88 amu, which corroborates well with the mono positive species **1a** (*m*/*z*: calcd 581.95 amu), shown in scheme 1. Immediately after the addition of TCC to the methanolic solution of **1** (complex:TCC = 1:100), the ESI-MS spectrum shows dramatic changes, and in this respect, two intermediates are feasible with the formation of **1b** (*m*/*z*: calcd 766.85 amu) and/or **1c** (*m*/*z*: calcd 748.84 amu), where TCC acts as a monodentate and a bidentate ligand, respectively, (Scheme 1).

Our ESI-MS spectrum clearly indicates **1c** (*m*/*z*: exptl 748.67 amu) as the better choice. To evaluate whether **1b** and **1c** might be real intermediates, we have performed a series of DFT calculations on the molecular models built by modifying the molecular crystal structure of **1** (Figure 1). The DFT-optimized geometries of **1c** and two rotamers, **1b** and **1b′**, are shown in Figure 5. All three geometries are optimized using the UB3LYP/SDD level, and the vibrational frequency calculations are performed to ensure that the optimized geometries represent the local minima and that there are only positive eigen values. The optimized structure of **1c** is characterized by a Ni−Ni distance of 3.372 Å, while 3.162 and 3.177 Å in the two rotamers **1b** and **1b′**, respectively. This, however, occurs at the expense of an increase in the structural distortion of the rotamer geometries, where the Ni−Ni bond vectors form an angle of 26.1 and 29.0°, respectively, for **1b** and **1b′** with the plane of the six-member arene rings, whereas this value reduces to 15.1° in **1c**. The computed zero-point energies of the two rotamers indicate that **1b** is about 8.89 kJ/mol lower in energy with respect to **1b′**. This extra-stabilization might be partly assigned to the presence of two

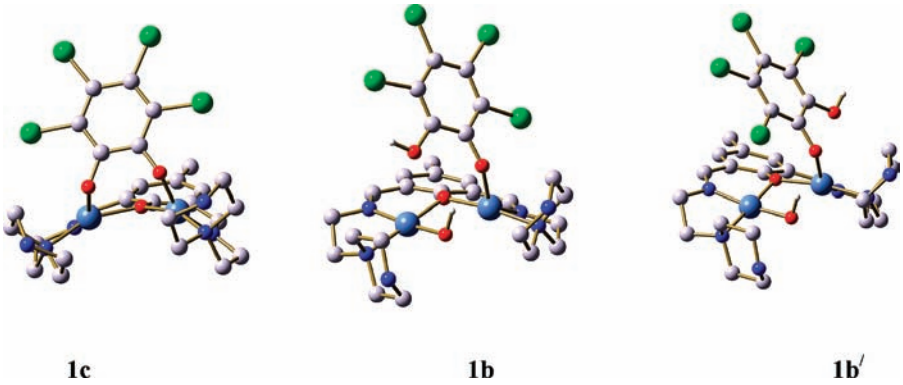

Figure 5. DFT-optimized structures of **1c** and two rotamers of **1b** and **1b/** (H-atoms are omitted for clarity).

Scheme 1. Possible Compositions of the Complex in Methanol (**1a**) and the Two Possible Adducts (**1b** and **1c**) upon Addition of TCC to a Methanolic Solution of Complex **1**

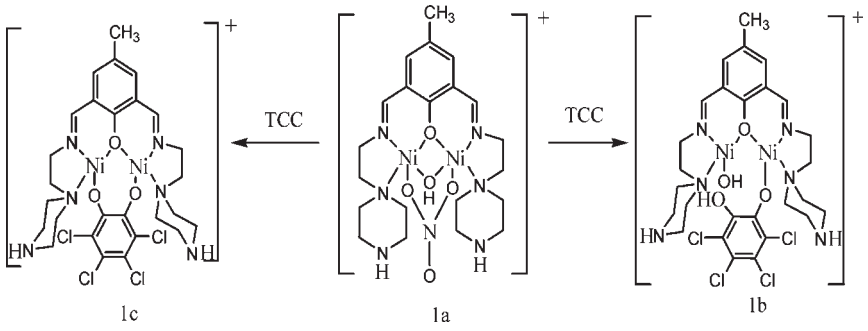

Scheme 2. An Alternative Possibility of the Generation of **1c** via **1b** on the Basis of a DFT Study

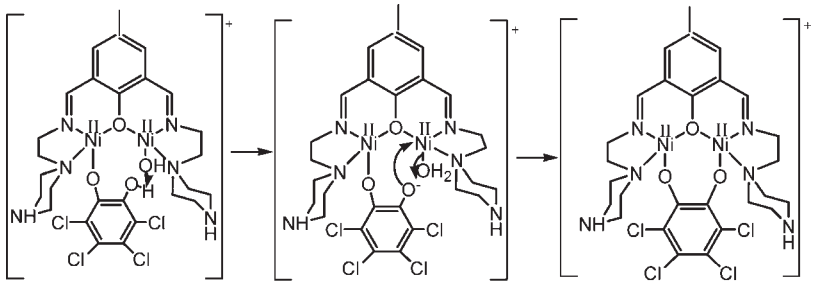

strong intramolecular H-bonds at 2.017 and 2.628 Å in **1b**, which elongates to 2.146 Å in **1b/**. The different stoichiometry of **1b** and **1c**, however, prevents us from assessing their relative stability. An examination of their optimized geometries, however, suggests that despite the difference in their Ni−Ni distances, the lower strain of the ligand associated to **1c** should favor the formation of this intermediate. Thus, our DFT calculations suggest that the TCC oxidation, catalyzed by complex **1**, most probably proceeds via the formation of an intermediate having bidentate coordination of TCC rather than monodentate coordination or that the formation of intermediate **1c** can take place via the formation of a secondary intermediate **1b** (Scheme 2). This conclusion agrees with that drawn from the ESI-MS measurements (vide supra).

The conversion of catechol to quinone is a two-electron oxidation process. Most of the investigators working with copper catechol oxidase model systems believe that the metal center redox participation is responsible for the catechol to quinone conversion,[30,31] though a recent point of view, based on theoretical calculations, advocates a radical pathway as the most reasonable alternative.[32] However, to date, no experimental evidence gives support to justify this proposition.

The electrochemical analysis of **1** in both the solvents, acetonitrile and methanol, is featureless, suggesting no preference for the nickel(II) ions is present in the complex to undergo reduction to nickel(I) or oxidation to nickel(III). Thus, from the above data, it is not possible to predict that the metal center redox participation is responsible for the catecholase activity of complex **1**. In

(30) Solomon, E. I.; Sundaram, U. M.; Machonkin, T. E. *Chem. Rev.* **1996**, *96*, 2563.
(31) Eicken, C.; Krebs, B.; Sacchettini, J. C. *Curr. Opin. Struct. Biol.* **1999**, *9*, 677.
(32) Siegbahn, P. E. M. *J. Biol. Inorg. Chem.* **2004**, *9*, 577.

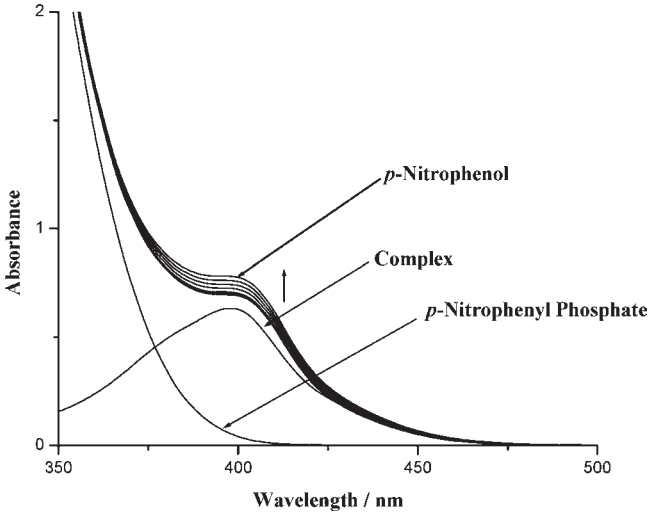

Figure 6. UV−vis spectrum (350−500 nm) of: (i) complex **1** (concn 1×10^{-4} M; in CH_3OH); (ii) changes in UV−vis spectra of complex upon addition of 100-fold PNPP in water−methanol (1:1 v/v) observed after a 5 min interval.

order to verify the other alternative, i.e., radical participation, we have performed an ambient as well as a low-temperature (−135 °C) EPR study, although EPR is not a good method to detect unpaired electrons in a transition-metal complex with a high D-value. However, we failed to detect any radical formation during our EPR experiment. Thus, at this moment, the actual mechanism through which complex **1** is exhibiting its extraordinary catecholase activity is not clear to us. This needs further extensive work, which is underway in our laboratory.

Phosphatase Activity. One of the criteria for a molecular species to function as chemical nucleases is to provide the H_2O/OH^- species as nucleophile. Since our complex possesses potential a nucleophile constituted by the metal-bridging hydroxyl group, it would be reasonable to explore the phosphatase activity of the complex. For this study, we have chosen PNPP as the test substrate. The reaction was followed UV−vis spectrophotometrically by monitoring the increase of the absorption band at 400 nm, due to the formation of PNP (Figure 6). The kinetics of the phosphatase activity was determined via the initial rates method by monitoring the increase of the product, *p*-nitriphenol, at 400 nm. The concentration of the substrate PNPP was always kept at least 10 times larger than that of the Ni(II) complex to maintain the pseudo-first order condition. All the kinetic experiments were conducted at constant temperature of 20 °C and monitored with a thermostat. Initially, a series of solutions of the substrate, PNNP, having different concentrations (1×10^{-3}−5×10^{-2} mol dm^{-3}), was prepared from concentrated stock solution of the substrate using methanol−water (1:1 v/v) as the solvent. Then 2 mL of such a substrate solution was poured into a 1 cm quartz cell kept in the spectrophotometer to equilibrate the temperature at 20 °C. A 0.04 mL (2 drops) of 5×10^{-3} mol dm^{-3} of Ni(II) complex in methanol was quickly added and mixed thoroughly to get an ultimate Ni(II) complex concentration of 1×10^{-4} mol dm^{-3}. The absorbance was continually monitored at 400 nm. The determination of the initial rates, as a function of the concentration of PNPP, reveals saturation kinetics with Michaelis−Menten-like behavior. By applying the GraFit32 program for enzymatic kinetics, K_m and V_{max} are calculated from the graphs (see Supporting Information), and catalyst's turn-over number, k_{cat} was determined by dividing V_{max} by the concentration of the complex ($k_{cat} = 7200\ h^{-1}$). To the best of our knowledge, the phosphatase activity of any nickel complex with our similar ligand system is not yet reported in the literature, and thus, in order to assess the catalytic efficiency of the present system, we compare its k_{cat} value with that of the analogous dicopper(II) complex. To our surprise, we noticed that the dicopper(II) complex is totally inactive in catalyzing the cleavage of the phosphate bond (see Supporting Information). The result indicates that the present dinickel(II) system is a more efficient catalyst than the dicopper(II) system under an identical environment, as far as phosphatase activity is concerned with PNPP as a substrate. Here, it is to note that the mechanism through which our dinickel(II) system catalyzes the phosphate-bond cleavage is not very clear to us, but we may assume that the Lewis acid (metal center) base (phosphate moiety) type interaction, as is proposed in the literature for zinc or copper complexes,[33] that catalyzed the phosphate-bond cleavage is operative also in our system.

An interesting remark is that recently polynuclear coordination complexes of copper, manganese, or nickel are in use as catalysts, especially for the oxidation of catechols, to know about the efficiency of a polynuclear system as catalyst in comparsion to an analogous di/mononuclear system.[34] The results obtained so far are interesting, but real working mechanisms are not yet identified.

DNA Cleavage Activity. On the basis of the encouraging result obtained in the hydrolysis of PNPP, we have decided to evaluate the influence of complex **1** toward nucleic acid degradation. Complex **1** is fluorescent, and its fluorescence intensity was observed to enhance in presence of DNA. We have exploited this phenomenon to determine the intrinsic DNA binding constant by applying the Benesi−Hildebrand model[35] (see Supporting Information), which evaluates K_{intr} as $2.69 \times 10^3\ M^{-1}$. To assess the DNA cleavage ability of complex **1**, supercoiled (SC) pGEM3Z plasmid DNA (200 ng for each set) was incubated with different concentrations of the complex in the presence of 10 mM tris buffer (pH 7) at 37 °C for 1 hour. The reaction was stopped with 1X DNA loading dye and resolved in 1% agarose gel. Upon gel electrophoresis of the reaction mixture, a concentration-dependent DNA cleavage was observed (Figure 7). The band intensity of the SC, the nicked circular (NC), and the linear (L) forms was measured through densitometric analysis (image quant software, Amersham Biosciences)

(33) Molenveld, P.; Engbersen, J. F. J.; Reinhoudt, D. N. *Chem. Soc. Rev.*, **2000**, *29*, 75 and references therein.

(34) (a) Alves, W. A; Cerchiaro, G.; Paduan-Filho, A.; Tomazela, D. M.; Eberlin, M. N.; Da Costa Ferreira, A. M. *Inorg. Chim. Acta* **2005**, *358*, 3581. (b) Majumder, A.; Goswami, S.; Batten, S. R.; Salah El Fallah, M.; Ribas, J.; Mitra, S. *Inorg. Chim. Acta* **2006**, *359*, 2375. (c) Ambrosi, G.; Formica, M.; Fusi, V.; Giorgi, L.; Micheloni, M. *Coord. Chem. Rev.* **2008**, *252*, 1121 and references therein.

(35) Carter, D. C.; Ho, J. X. *Adv. Protein Chem.* **1994**, *45*, 153.

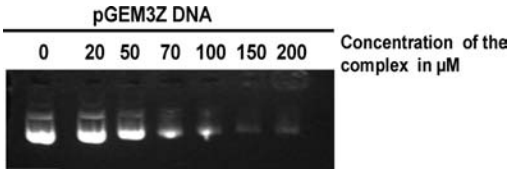

Figure 7. Gel electrophoresis showing the cleavage of SC pGEM3Z plasmid DNA (200 ng in base pair) with different concentrations of complex **1**, in presence of 10 mM tris buffer (pH 7) at 37 °C for 1 hour.

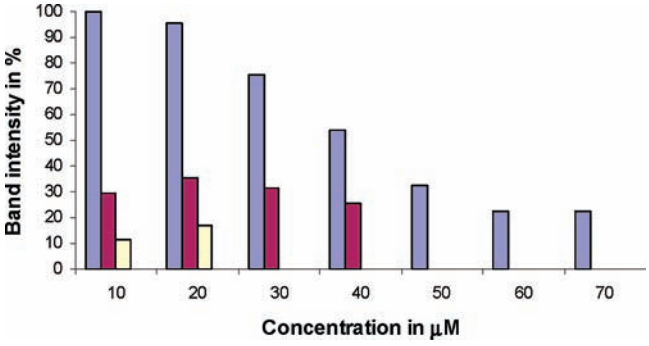

Figure 8. Relative amounts of the different DNA forms in the presence of increasing concentration of complex **1**; SC is violet; NC is brown; and L is yellow.

and plotted against an increasing concentration of the complex (Figure 8).

The densitometric analysis data showed that the complex can cause the cleavage of the SC DNA, even at a 20 μM concentration. The Figure shows a decrease of the SC percentage and an increase of both the NC and L forms, with respect to the control. Interestingly at a 50 μM concentration, the SC form is diminished, as expected, but both the NC and L forms are also decreased. This particular trend is observed also at higher concentrations. These experimental facts may be explained in the following way: Complex **1** causes the conversion of SC to NC and L, which were finally cleaved to small oligonucleotides by nonspecific cleavage at various sites. At very low concentrations of the complex, the rate of the reaction is slow, and the intermediate formation of the nicked and linear forms may be observed but at a higher concentration of the complex; the rate of conversion of the DNA to small oligonucleotides is too high, and we can only observe the decrease in the SC form without increasing NC and/or L. Reports on DNA cleavage by nickel(II) complexes are very scanty.[36] The available data reveal that two mechanisms likely to be involved in DNA cleavage are the hydrolytic cleavage and free radical mechanisms. In our case, the DNA cleavage was observed to inhibit, to a significant extent, when the reaction was carried out with 150 μM of the complex in the presence of DMSO (hydroxyl radical scavenger). The use of NaN_3, as a singlet oxygen scavenger, did not inhibit the DNA cleavage (Figure 9). The above facts reveal that the ability of complex **1** to generate hydroxyl radicals is most likely responsible for the cleavage to DNA.

The use of metallonucleases in the living cells as DNA foot-printing agents suffers the deadlock, as most of them

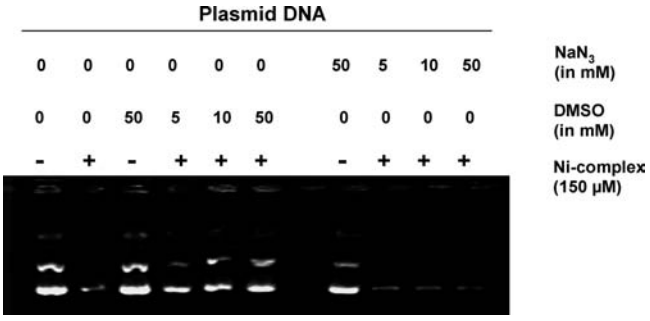

Figure 9. Lane 1: pGEM3Z plasmid DNA (200 ng in base pair). Lane 2: pGEM3Z plasmid DNA (200 ng in base pair) with 150 μM of the complex **1** alone. Lanes 4−6: pGEM3Z plasmid DNA (200 ng in base pair) with 150 μM of the complex **1** in the presence of radical scavenger DMSO. Lanes 8−10: pGEM3Z plasmid DNA (200 ng in base pair) with 150 μM of the complex **1** in the presence of NaN_3. The pGEM3Z plasmid DNA was also incubated with DMSO (lane3) and NaN_3 (lane7) alone to show that these scavengers do not have any effect on the DNA.

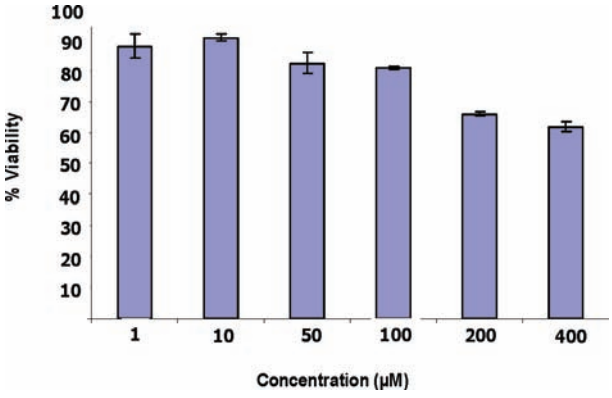

Figure 10. The effects of complex **1** on VERO cells' viability. Cells were treated for 30 h with the compound at the indicated concentrations. Cell viability was estimated by a MTT assay, as reported in the Experimental Section. Data are expressed as the percentage of viable cells with respect to untreated controls.

show activity only in the presence of excess of an external reluctant and dioxygen. Since our complex can bind and cleave DNA by a self-activating mechanism, its application in site-specific recognition of DNA, even in in vivo conditions, should be very promising.

Bioactivity. To investigate this potentiality, the complex was tested for its effect on the viability of living cells using a MTT assay.[37] VERO (a monkey kidney cell line) and A549 (a carcinomas human alveolar basal epithelial cell line) cells were used for the detection of cytotoxicity, and the results indicate that, at moderate concentrations, (200−400 μM) the complex shows around a 40% decrease in the viability of VERO cells (Figure 10), which may be a consequence of the DNA cleavage activity of the same. Also the effect of this complex upon the carcinoma cell line, A549, was similar.

Conclusions

In conclusion, complex **1**, the first ever example of this kind, possesses an inherent property exhibiting versatile catalytic activities of biological significance. The catecholase activity of complex **1** is observed to be largely influenced by

(36) Benelli, C.; Dei, A.; Gatteschi, D.; Pardi, L. *Inorg. Chem.* **1989**, *28*, 1476.

(37) Mosmann, T. *J. Immuno. Methods* **1983**, *65*, 55.

the nature of the solvent. In a methanol medium, the complex shows excellent catecholase activity not only with easily oxidiazable 3,5-DTBC but also with TCC, a substrate whose oxidation catalyzed by any nickel(II) complex is not known to date, whereas in the acetonitrile medium, it becomes inactive, even in oxidizing 3,5-DTBC. An UV−vis spectral study clearly shows TCC oxidation catalyzed by complex **1** proceeds through the formation of an intermediate, whereas for 3,5-DTBC, the intermediate, if at all formed, is too unstable to detect. ESI-MS measurements and DFT calculations suggest that the coordination mode of TCC in that intermediate is a bidentate bridging type rather than a monodentate. The complex **1** also exhibits interesting DNA cleavage activity, most probably through a hydroxyl radical pathway. This very property may be crucial for its possible applications in site-specific recognition of DNA, even in in vivo conditions, as well as for a promising anticancer drug, as is evident from the bioactivity study of the complex. Generally, nickel compounds are considered as moderately cancerous. However, the report presented in this communication suggests further extensive investigation with a similar nickel(II) system to get a breakthrough.

Acknowledgment. We are thankful to Dr. P. S. Mukherjee, IISc, Bangalore, India, for his help on variable-temperature magnetic susceptibility measurement and for many fruitful discussions. The generous help of Mr. Bijan Pal, Research Scholar, Department of Chemistry, University of Calcutta, India, to determine the DNA binding constant is also duly acknowledged.

Supporting Information Available: X-ray crystallographic data in CIF format of **1**, IR spectrum, UV−vis spectroscopic and kinetic data, and ESI-MS spectra for **1** and its TCC adduct (intermediate) in methanol, CV for **1** in methanol, DNA cleavage and MTT assay, emission spectra, and determination of DNA binding constant. This material is available free of charge via the Internet at http://pubs.acs.org.